JOURNAL OF NANO- AND ELECTRONIC PHYSICS
Vol. **18** No 4, 04029(10pp) (2026)

ЖУРНАЛ НАНО- ТА ЕЛЕКТРОННОЇ ФІЗИКИ
Том **18** № 4, 04029(10cc) (2026)

OPEN ACCESS

REGULAR ARTICLE

wxAMPS Simulation of Electronic Transport Mechanism in Intrinsic and Doped Nanocrystalline Silicon Thin Films

M. Chahi[1,2], A. Gharou[3], H. Nehmar[4,*], M. Kasdi[3], H. Benhabara[4], A. Bouhekka[3,4]

[1] *Laboratoire de Génie Electrique et Matériaux LGEM Ecole Supérieure en Génie Electrique et Energétique ESGEE d'Oran, Oran, Algeria*
[2] *Institute of Nature and Life Sciences, Tissemsilt University – Ahmed Ben Yahia ELWancharissi, P.B. 182 Bougara Road, 38000 Tissemsilt, Algeria*
[3] *Department of Matter Sciences, Faculty of Sciences and Technology, Tissemsilt University – Ahmed Ben Yahia ELWancharissi, P.B. 182 Bougara Road, 38000 Tissemsilt, Algeria*
[4] *Laboratoire de Physique des Couches Minces et Matériaux pour l'Electronique – LPCMME, Université Oran 1 Ahmed Ben Bella, B.P. 1524, El M'naouar 31100 Oran, Algeria*

(Received 10 February 2026; revised manuscript received 15 August 2026; published online 21 August 2026)

The main objective of this research is a numerical investigation of the transport properties in hydrogenated nanocrystalline silicon thin films for solar cells applications using the wxAMPS software tool. The simulated samples were fabricated at 100 °C using radiofrequency magnetron sputtering (RFMS) method with RF power 220 W, a gas mixture of 30 % of argon and 70 % of hydrogen under a total pressure of 3 Pa and the target – sample holder distance, fixed at 70 mm, were maintained constant for the three categories intrinsic, phosphorus doped and boron doped films at deposition times of 3 and 30 minutes. The simulation carried out in this research, is based on a layer of nanocrystalline silicon that was constructed using successive and alternative crystalline and amorphous thin layers where their total number is depending on the thickness of the considered sample. The electronic transport mechanism is studied and findings clearly demonstrated that doped and undoped samples have different activation energy (E_a) which obviously illustrates the crucial role of doping. The E_a is less than 0.2 eV for all the simulated samples strongly indicating a hoping transport mechanism. These results were compared to experimental and previous works where a good agreement was observed.

Keywords: Nanocrystalline silicon, wxAMPS software, Dark conductivity, Activation energy, Hopping, Simulation study.

DOI: 10.21272/jnep.18(4).04029 PACS numbers: 72.80.Jc, 73.63.Bd

1. INTRODUCTION

Low-temperature synthesis of nanocrystalline silicon thin films (nc-Si: H) was discovered by Veprek and Marecek in 1968 [1]. During the last few years, researchers have extensively studied the nc-Si: H for different energy applications since the early 1990s, including thin film solar cells, thin film transistors, light emitter devices, photodetectors, synaptic devices as well as nonvolatile memories [2, 3]. They exhibit superior doping efficiency, higher mobility and low absorption compared with those of hydrogenated amorphous silicon thin films [4] and high stability under illumination as well as higher conductivity [5]. A variety of growth techniques have been used to prepare these types of silicon. These methods include the ion implantation of silicon (Si) into dioxide silicon (SiO_2) films, deposition of thin films of Si nanocrystals by sputtering [6], plasma enhanced chemical vapor deposition (PECVD) [7] or low-pressure chemical vapor deposition techniques (LPCVD) [8], aerosol deposition of Si nanocrystals [9] and radio frequency magnetron sputtering at low temperature (RFMS) [10, 11]. Interestingly, an impurity such as boron significantly influences the crystallinity [12] while low-temperature deposition is needed for better one [13, 14].

The nc-Si: H material properties are not well understood because of the complexity of its structure. The conventional structural picture of nc-Si :H materials includes crystalline nano-grain with sizes around 5 to 20 nm [15, 16] forming columns with a diameter of around 200 nm, dependent on the substrate temperature [17], tending to grow perpendicular to the film surface, hydrogenated amorphous often called 'tissue' and voids are also found within this material [12, 18, 19]. A difficult characterization of this material is due to the heterogeneous structure because some concepts in homogenous materials such as crystalline and amorphous semiconductors may not be applicable for nc-Si:H due to its band gap which is not well defined or characterized [19].

The heterogeneous structure of this kind of material and its complex configurations make very difficult all attempts to correlate the structure properties with electrical transport mechanism [12, 20]. The conduction mechanisms are discussed in different models that involve

* Correspondance e-mail: nehmarmora@gmail.com

Cite this article as: M. Chachi et al., *J. Nano- Electron. Phys.* 18 No 4, 04029 (2026) https://doi.org/10.21272/jnep.18(4).04029

potential barriers at grain boundaries, tunneling, hopping, and percolation [21]. Differences and similarities between intrinsic and doped nc-Si:H conductivity were observed and these are also explained on the basis of recently published studies [22].

It will be useful to start with a brief discussion of the basic problem: Macroscopic measurements can clarify the dominant transport mechanism, but not the specific network responsible for the conduction. In other words, macroscopic transport measurements can indicate how but not where (i.e., in which phase of the film) the conduction takes place [18]. The conductive atomic force microscopy (C-AFM) studied by Rezek et al., [23] and scanning tunneling microscopy (STM) investigated by Ross et al., [24] have shown that conduction takes place through the individual crystallites, consistent with macroscopic data and in agreement with the relatively high conductivity of those crystallites. D. Azulay et al., [25] have suggested that transport takes place in some disordered silicon tissue, rather than via the crystallites. The discrepancy between the microscopic results of these two groups has been explained by taking into account the different procedures of growth of the Si films: the samples investigated by Azulay et al. were grown under high vacuum, while those studied by Rezek et al could have contained considerable oxygen concentrations that could yield unintentional doping of the layers [18]. Therefore, further investigation of the transport mechanism in nc-Si: H cell is still necessary.

For a better understanding of the physical origins of conduction behaviors in the nc-Si: H, it involves to take into consideration the possible conduction mechanisms between two phases: two crystallites in large grain (column), between large crystalline grains (potential barrier between them) and between crystalline/amorphous which depicts the potential barrier of the heterojunction [26]. The main problem regarding such composites is then the determination of the dominant electrical conducting network and the related transport mechanism as described for microcrystalline silicon by [27, 28]. For this propose, we attract a considerable attention on the simulation study of nanocrystalline silicon based on simulation model described in previous published works [28, 29], as well as the seto's model which is well described in [30]. The conduction mechanisms occurring in these cells will be investigated with a developed version of AMPS program called wxAMPS [31] and more details are given in the next section. The simulation results will be compared with the experimental ones studied by Benlakehal [12].

2. EXPERIMENTAL AND MODELING

In this work, the simulated samples were fabricated and studied experimentally [12] using radiofrequency magnetron sputtering (RFMS) method with RF power 220 W, a gas mixture of 30 % of Argon and 70 % of Hydrogen under a total pressure of 3 Pa and the target – sample holder distance, fixed at 70 mm, were maintained constant for the samples. The deposition rate of 3 and 30 minutes were tested. They investigated film conductivity via several technological parameters, such as doping type (p and n), deposition rate and crystalline grain size and comprehensive models current transport. The size shape and density of crystallites embedded in the amorphous matrix of the all samples were determined by Raman spectroscopy. For the films deposited during 30 minutes at 100 °C, the Raman spectra indicated the important presence of the crystallites in the samples which is described in detail in [12, 32].

Structurally, we believe that a nc-Si: H material is composed of crystalline silicon grains separated by amorphous silicon grains boundaries (GBs). Conduction through a nc-Si film is strongly affected by potential barriers at the GBs, associated with the large density of trapping states caused by defects at the GBs [33].

The structure of nanocrystalline silicon makes the experimental study of the optical and electrical properties of the resulting solar cell more complex. For further optimization of the solar cell performance, a good understanding of the contribution of each layer and interface to solar cell performance is imperative. These contributions can be investigated by numerical simulation in order to complement the limitations of experimental work.

In a real polycrystalline material, the crystallites have an unequally distributed size, irregular shapes and orientations [3]. It is composed of small crystallites of size about 30 nm joined together by a few disordered atomic layers, which results in carrier trapping at the grain boundary (GBs), creating a potential barrier [30]. The adopted model to explain the conductive properties of polycrystalline material, originally proposed by Seto, called the grain boundary trapping (GBT) model [34,35]. It Considers a one-dimensional chain of identical nc-Si having a grain size (D), where the (GB) thickness is small relative to the grain size, as shown in Fig. 1.

In this article we have applied directly a (GBT) model for nc-Si: H films which identifies the conduction of nc-Si: H as a thermionic emission and thermal-assisted tunnelig processes using wxAMPS software.

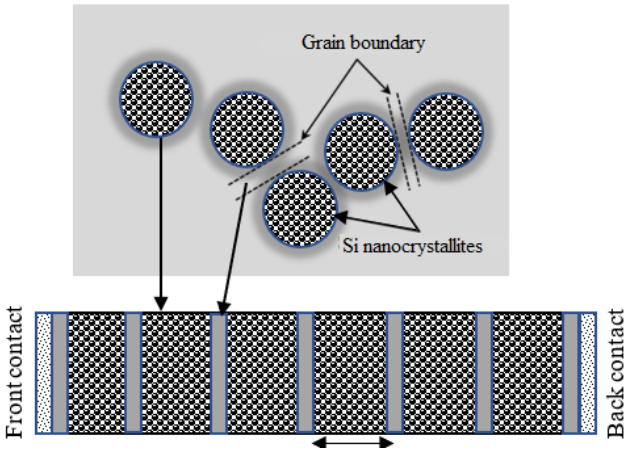

Fig. 1 – Simulation model following the Seto and Le Comber models

According to the GBT model, we assumed in the first approximation an alternating stack of a-Si:H (GBs) and c-Si (crystalline grains). From one electrode to other, during their emotion, electrons cross crystalline and amorphous phases that can support this model. In fact, the growth of the material is perpendicular to the substrate and the displacement of the charge carriers can be in the transverse or longitudinal direction according

to the electrodes disposition. In both cases the simulation model of electron transport is the same. The number of films is fixed and the size of crystalline films is assumed to have the same value and varies between 5 nm to 20 nm depending on their volume fraction whereas the amorphous grain size varies between 2.5 nm till 7 nm [36]. In our study, the crystalline fraction (X_C) will be calculated by the following formula:

$$X_c = \frac{\sum crystalline\ layer\ thickness}{\sum crystalline\ layer\ thickness + \sum amorphous\ layer\ thickness} \quad (2.1)$$

We have changed the crystalline fraction by varying thickness of crystalline silicon layers to examine the influence of the electrical and structural properties of volume crystalline fraction on conduction mechanisms. In order to compare the experimental results with those simulated, we must take into consideration the crystalline volume fraction measured by Raman and ellipsometry spectroscopies [12].

Three categories (intrinsic, n doped and p doped), with their corresponding X_C, of samples were prepared at T = 100 °C and times of 3 min and 30 min as indicated below:

- intrinsic films: i03min (X_C = 0, d = 43 nm) and i30min (X_C = 74%, d = 395 nm)
- n doped films: n03min (X_C = 35%, d = 47 nm) and n30min (X_C = 72 %, d = 428 nm)
- p doped films: p03min (X_C = 38%, d = 43 nm) and p30min (X_C = 73,5 %, d = 433 nm)

The wxAMPS-1D tool is an improved version of AMPS, and was developed by Prof. Angus Rockett and Dr.Yiming Liu at the university of Illinois at Urbana Champaign, in collaboration with Nankai University of China. It is a substantially new solar cell simulator for modelling one dimensional devices composed of various materials. This modified version accepts the same input parameters and ensures the similar physical principles and numerical descriptions of defects and recombination as AMPS [37, 38]. wxAMPS is written in C++ and includes a number of revisions to the basic algorithm [38]. In addition, wxAMPS version has the capabilities to include several different tunnelling principles: trap assisted, intra-band, and band-to-band mechanisms [31, 39]. It solves simultaneously the Poisson equation and the electron and hole continuity equations by using the method of finite differences and the Newton-Raphson technique.

The continuity equation in one dimension along the x-axis for both electrons and holes can be written as:

$$\frac{\partial n}{\partial t} = \frac{1}{q}\frac{\partial J_n(x)}{\partial x} + \mathcal{G}_n - \mathcal{R}_n \quad (2.2)$$

$$\frac{\partial p}{\partial t} = -\frac{1}{q}\frac{\partial J_p(x)}{\partial x} + \mathcal{G}_p - \mathcal{R}_p \quad (2.3)$$

where $\mathcal{G}_n$ ($\mathcal{G}_p$) and $\mathcal{R}_n$ ($\mathcal{R}_p$) are the generation and recombination rate of both electron and holes respectively. $J_n$and J_p are the electron and hole current densities.

Poisson's equation links free carrier populations, trapped charge populations, and ionized dopant populations to the electrostatic field present in a material system. In one-dimensional space, Poisson's equations are given by:

$$\frac{d}{dx}\left(-\varepsilon(x)\frac{dV}{dx}\right) = q[p(x) - n(x) + N_D^+(x) - N_A^-(x) + p_t(x) - n_t(x)] \quad (2.4)$$

Where the electrostatic potential V and the free electrons n, free holes p, trapped electrons n_t, and trapped holes p_t, as well as the ionized donor like doping N_D^+ and ionized acceptor like doping N_A^- concentrations are all functions of the position coordinate x. Here, ε is the permittivity and q is the magnitude of the charge of an electron.

The crucial point in modelling a device based on nc-Si:H material is to define the role played by the boundary regions between the crystalline grains and the amorphous matrix. In this transition regions it is supposed to be localized a high concentration of defects in the lattice structure. If the distance between two adjacent grains is large enough this region could be treated similarly to a heterojunction. To distinguish one transport mechanism from the others, we employ the well-known general junction rectification model [40] to clarify the relation between the current and the applied forward bias voltage.

We have to devise different mathematical models which are able to describe the important physical phenomena for a particular situation or for particular device. Moreover, since in some cases we are not interested in all the available physical information, we need simpler models which help to reduce the computation cost in the numerical simulations [41].

Based on the approach consideration of nc-Si:H cells as a diode, [19] the dark JVT characteristics can be given by the following formula:

$$J = J_0\left[exp\ \left(\frac{qV}{nkT}\right) - 1\right] \quad (2.5)$$

Where k is the Boltzmann constant, n is the ideality factor and J_0 is the saturation current density. In this case, a very good phenomenological approximation for most diode and solar cells even though the complicated recombination is given by the following relation [19, 42]:

$$J_0 = J_{00} exp\ \left(-\frac{E_a}{kT}\right) \quad (2.6)$$

$$log\ J_0 = log\ J_{00} - \frac{E_a}{kT} \quad (2.7)$$

Where E_a is the activation energy.

The above equation has the form of the equation depicting a straight line $y = A + Bx$. It is observed that the nc-Si:H is biphasic material consisting the crystalline and amorphous silicon. Accurate modelling and simulation of thin film solar cells based on nc-Si:H requires models that describe the specific material parameters based on their component such as the amorphous and crystalline phases.

In crystalline semiconductor carrier transport takes place in extended states inside the energy bands and the high carrier mobilities are limited by scattering at phonons or impurities. The gap states appear as isolated states and electronically communicate with the energy bands only. In our numerical simulation, the atoms of crystalline silicon are well organized which is reflected by the absence of band tails in the gap but there is no perfect crystalline structure and the existence of some vacuum create localized states in the middle of the gap.

Therefore, the density of state (DOS) of crystalline silicon can be parameterized with a donor and an acceptor Gaussian distribution located at midgap with very low value [21, 28]. In an amorphous semiconductor disorder causes localization at the band edges and tails of localized states extend deep into the energy gap. The localized and extended states are separated by mobility edges which for the transport mechanism, at higher temperatures, play a role quite similar to the band edges in crystalline semiconductors [21]. In the present simulation, we need an initial set of parameters for all the properties of the grain boundaries (amorphous matrix) and the grain crystalline silicon materials like band gap, electron affinity, doping, mobilities, gap defect states distribution in the bulk and at interfaces, B and P doped concentration. The input parameters and thickness for each layer adopted in our simulation model were derived from the properties of the reported materials in the literature.

2.1 Defect State Distribution of c-Si and a-Si

2.1.1 Electrical and Defect (Middle Gap) Parameters

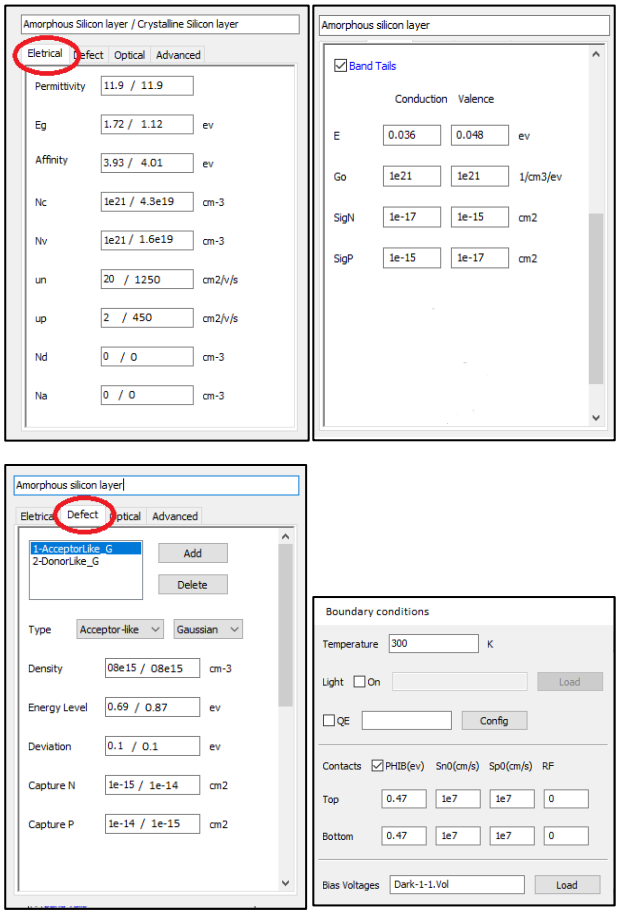

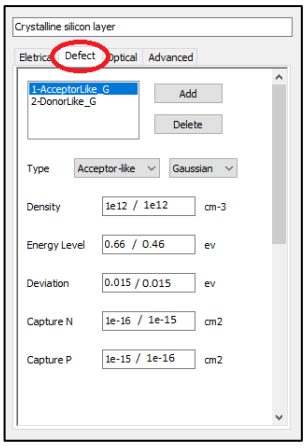

Fig. 2 – Set parameters of simulation

PHIB: represents the height barrier in the contact between the metal and semiconductor.
PHIB = $\phi_M - \chi_S$, where ϕ_M is the work function of the metal and χ_S is the electronic affinity of semiconductor (eV).
SN: Surface recombination speeds of electrons (cm/s).
SP: Surface recombination speeds of holes (cm/s).
Bias voltage: Applied voltage on our samples.

3. RESULTS AND DISCUSSION

3.1 Current – Voltage Characteristics

The electrical characteristics study of any solar cells under dark conditions allows one to determine the device parameters. It is the easy way to estimate its quality and performance.

From the solution provided by the wxAMPS simulation, output such as the dark current voltage characteristics under different temperature values, shown in Fig. 3a, which reflects a clear behavior governed by the Eq. (2.5) where the curves exhibit approximately a linear behavior at a given temperature. We found that the dark current density-voltage characteristics fit the standard diode ones. In this study, many more nc-Si:H structures were simulated.

Parameters extraction is a fundamental process to evaluate the performance of photovoltaic (PV) devices. The obtained parameters can be used not only to predict the behavior of solar cells but also to obtain essential information about device performance and efficiency.

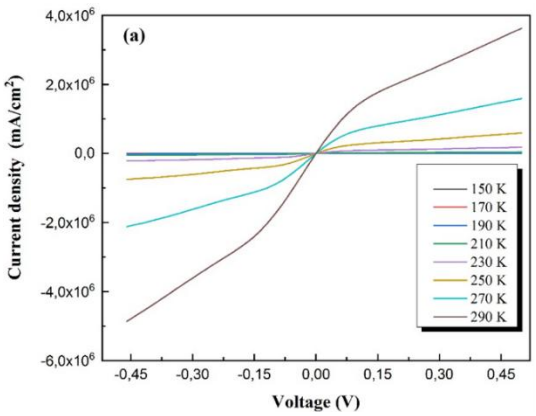

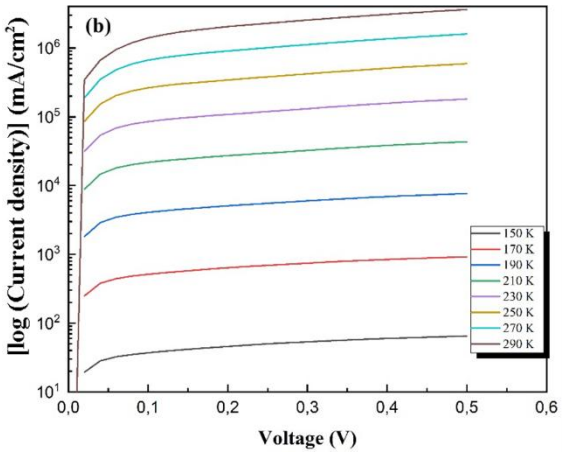

Fig. 3 – (a) An example of current density voltage characteristics of nanocrystalline silicon (n30min100) under dark conditions at different temperature values and (b) (Log(J) vs V)

One of these parameters is the pre-exponential factor J_0 Eq. (2.5), deduced from the logarithm of the dark current density versus voltage at different temperatures (JVT) characteristic as shown in Fig. 3b. The J_0 of the samples in the model are the y-intercept value of the linear regression plot of the Eq. (2.5).

One of the most important parameters that we are looking for is the activation energy which is strongly affected by the structure and the type of the considered material.

3.2 Conductivity Activation Energy

The activation energy (E_a) determination procedure is shown in Fig. 4, which represents the log of J_0 as a function of 1/KT. The slope of the linear fitting indicates the $E_a$while the interception with the y axis represent the pre-exponential factor (J_{00}) in Eq. (2.6). This method was applied to the rest of samples to calculate their corresponding activation energies. We found that only one electronic transport mechanism is dominated for all samples, Mott variable-range hopping (Mott-VRH) occurs at the temperature range of 270 to 450 K as reported by [43].

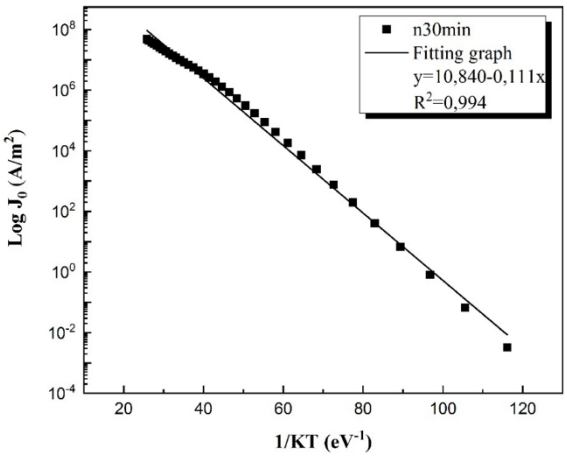

Fig. 4 – An example of n30min sample illustrating fitting procedure to determine the activation energy of the samples

3.2.1 Undoped nc-Si:H Samples

The intrinsic samples (undoped) were deposited without any impurities during 03 min and 30 min and their activation energies (E_a) are simulated and the results are given in Fig. 5. This latter clearly demonstrates that both samples have an E_a less than 0.13 eV. The sample i03 min is fully amorphous structure. Its small activation energy E_a = 0.100 eV, simulation value, indicates that the majority of the charge carriers reside in localized states existing in the band gap and never need to be excited directly to conduction band. This is often the case for amorphous materials in this range of temperature [44]. The states localized around the Fermi level is the dominant process. Experimentally, this small value can be interpreted by the presence of oxygen atoms in the films which seem to play an important role in the electrical conduction mechanism [12]. The deposition time, 30 min, gave a complex material, nc-Si:H, containing a nanocrystal embedded in amorphous tissue. This material type has a 74 % of crystalline fraction and very important defects located in the amorphous tissue which is assumed as grain boundaries in our simulation model. The E_a = 0.129 eV is confirmed that the grain boundary plays an important role in the carrier transport process in un-doped nc-Si film which can be well described by the previously proposed model.

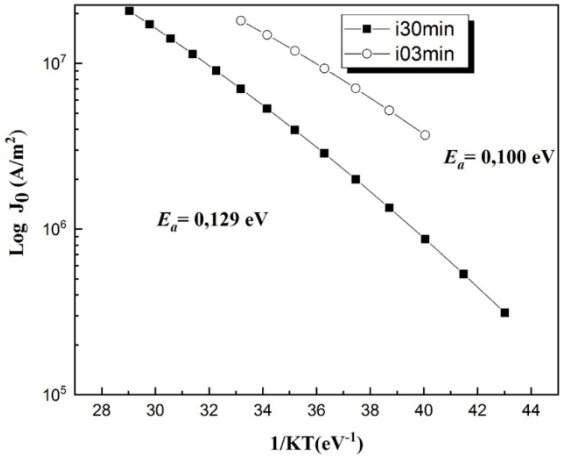

Fig. 5 – Simulated variation of Log $J_0(T)$ as a function of the inverse of KT, in temperature range 270-400 K obtained for intrinsic silicon thin films deposited at 3 min and 30 min T = 100 °C

It is possible, however, to modify the conductivity of the semiconductor solar cells over many orders of magnitude. Among conventional methods, doping is a key factor in improving the performance of semiconductors, considered as an effective way for the practical use of intrinsic ones [45, 46]. To increase the electron density in our samples an impurity such as phosphorus (P) is substituted for some of the Si atoms [47]. It was reported that introducing a great deal of P atoms in the silicon matrix can be helpful for the formation of four-coordination, especially after annealing, leading to an increase in the structural ordering of the samples and in turn promotes crystallization [3].

Similarly, the introduction of trivalent impurity such as boron B will introduce localized states just above the valence band called acceptor levels where holes are the

majority carriers. However, such doping is accompanied by an increase in the bond-angle and bond-length perturbations. The B atoms incorporated in the films cause the distortion of the short range orderness, which may produce a slight reduction of crystallinity in B doped nc-Si:H films [45]. Therefore, study on the properties of doped nc-Si:H is necessary and important [2, 45].

3.2.2 *n*-type nc-Si:H Samples

As indicated in the experimental work [12], these samples were deposited using phosphorus impurities, during two different periods of time as the intrinsic ones. The conductivity activation energy of nc-Si:H films prepared at period 30 min is significantly reduced after P doping compared with those prepared at period 03 min as illustrated in Fig. 6.

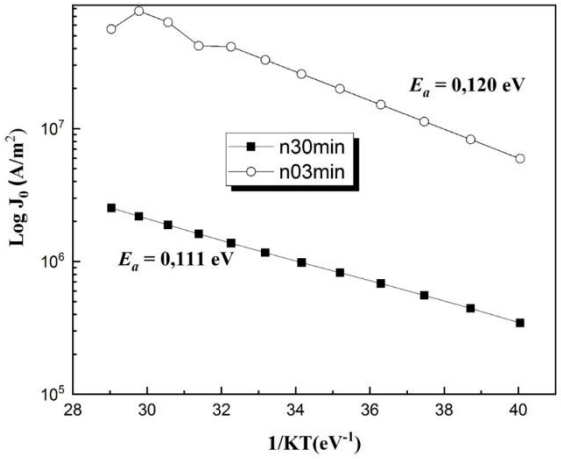

Fig. 6 – Simulated variation of Log $J_0(T)$ as a function of the inverse of KT, in temperature range 290-400 K obtained for n doped nanocrystalline silicon thin films deposited at 3 min and 30 min at T = 100 °C at a concentration of phosphorus N_D = 50 ppm

The majority of carriers, in these samples, are electrons and the curves, in Fig. 6, are well fitted by the Eq. (2.6). The calculated activation energy, by simulation, of both samples is around 0.1 eV which strongly means that doping has a crucial role in effecting the electrical properties of the films. The comparative study of both n-doped (n03min, n30min) and intrinsic i30min nc-Si:H thin films shows a slight decrease of E_a values in the presence of phosphorus impurities. However, according to [48,49], at certain range, the phosphorus doping ratio enhances the film conductivity. The decrease in E_a suggests that the structure becomes more crystalline with increasing dopant concentration, as discussed experimentally in [3,45], hence generating electron hole pair will be easy with small energy. The weak values of E_a might be due tothe fact that the Fermi level is shifted near the conduction band by defects in the distorted network at the transition between crystallites and the surrounding amorphous matrix as it suggested by [10].

3.2.3 *p*-type nc-Si:H Samples

As confirmed in the experimental work [12], these samples were elaborated using boron impurities, at two different periods of time as the previous ones. After B doping, the E_a of nc-Si:H films prepared at 30 min is significantly increased compared to those prepared at 03 min as shown in Fig. 7.

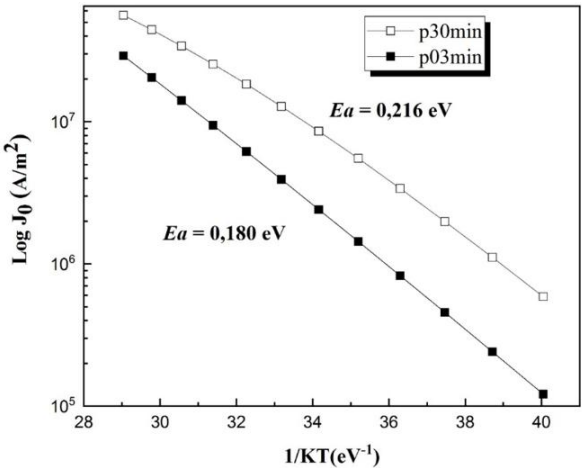

Fig. 7 – Simulated variation of Log $J_0(T)$ as a function of the inverse of KT, in temperature range 290-400 K obtained for p doped nanocrystalline silicon thin films deposited at 3 min and 30 min at T = 100 °C with concentration of boron N_A = 100 ppm

The linear fit, represented in Fig. 7, reveals that the activation energy of both samples is around 0.2 eV, which strongly implies that the doping has an important effect on the electrical properties of the films, where it will be easy to generate electron hole pair with small energy but still bigger than that of P doped nc-Si:H. The value of E_a suggests also that the Fermi level moves from its intrinsic position towards the top of the valence band due the doping effect [2]. The E_a values of B doped nc-Si:H is increased compared to those of P doped and intrinsic nc-Si:H films. At the end, the crystallinity of the films decreases when the doping concentration of the Boron increases. Such behavior could explain that the large amorphous fraction produces a large disorder material leading to low dark conductivity [43,49].

Our simulation results are in good agreement with the previous experimental findings relative to doped and undoped nc-Si:H [12], as illustrated in the Table 1.

Table 1 – Activation energy comparison between simulation and experiment results

Sample name	Thickness (nm)	Crystalline fraction X_C (%)	Activation energy E_a (eV)	
			Simulation.	Exp [50]
i03min	45	00.00	0.100	0.120
i30min	450	74.00	0.129	0.180
n03min	45	35.00	0.120	0.120
n30min	450	72.00	0.111	0.140
p03min	45	38.00	0.180	0.110
p30min	450	73.50	0.216	0.200

From Table 1, it is clear that E_a is in the range 0.1-0.2 eV. These values are clearly different from a typical recombination diode and must be explained by other mechanisms [48]. Our samples are considered as a mixed semiconductor phases. The grain boundaries act as potential barriers for charge transport and play a pivotal role in determining charge transport properties of nc-Si: H [36].

According to some authors [51, 52], the grain boundary region mainly controls the charge transport at low temperatures, and the electrons are able to surmount the lower barrier by tunneling. The logical and reasonable E_a values clearly support the hypothesis and supposition that at the grain boundaries, the carriers transport (current) is dominated by the tunneling process. For this kind of materials, the greatest crystallinity leads to the thickness of smallest barrier and therefore to a larger tunnel effect [53]. Mott suggested that at low temperature the most frequent electron hopping between localized sites would not be essentially to the nearest neighbor, because phonons may not have enough energy for transferring to a nearest neighbor atom at higher energy level and the charge carrier possibly hops from a neutral atom to another same one situated, many inter atomic distance away, with the same energy level [54]. The tunneling transitions (hopping) of carriers from occupied to unoccupied localized states, called variable range hopping (VRH), and one or more phonons may be involved in the hopping process [54]. Electrons can move by hopping from a localized state to another one under a weak thermal activation (low activation energy) which strongly satisfies the Anderson´s criterion [55].

It has been pointed out that the increase in conductivity could be due to the increase in the portion of hopping conduction through defect states associated with the impurities [56]. A special attention has been paid to the effect of the presence of B and P atoms on the structural and electrical properties. Table 1, obviously indicates a remarkable comparison of our results obtained for intrinsic and doped samples deposited at the same period of time. Introducing P impurities in nc-Si:H leads to a decrease in E_a, which increases in the case of B doped. The above-mentioned results could be explained by the importance of grain boundaries (amorphous layers) that play the role of potential barriers. Therefore, they impede the motion of free carriers by trapping [35]. Such grain boundaries have a large number of defects which can trap the carriers and form the electrically charged states. These latter impede carriers' motion between different crystallites thus mobility is reduced.

3.3 Energy Band Diagram

The interfaces between the layers of the solar cell play a key role due to the electron energy level differences and their relative alignment. This latter describes built in electric fields that appear across material junctions which illustrate the drift currents preferred direction and suggesting potential tunnelling effect. This indicates a clear idea and a deeper understanding to the workings mechanisms of the device [57].

Considering the present nc-Si:H films surface with less amorphous components and potential energy barriers due the GBs between crystalline regions. Depending on the crystallinity, we take into account the two types of the tunnel junctions created between adjacent crystallites and that produced between adjacent crystallites columns [58]. The difference in energy band gaps creates valence and conduction band offsets which act as barriers to carrier transport. The simplified energy band diagram carried out by simulation is plotted in Fig. 8, where E_C and E_V represent the edge of the conduction and valence band, while the E_{fn} and E_{fp} are the quasi-Fermi levels, E_b is the potential barrier height.

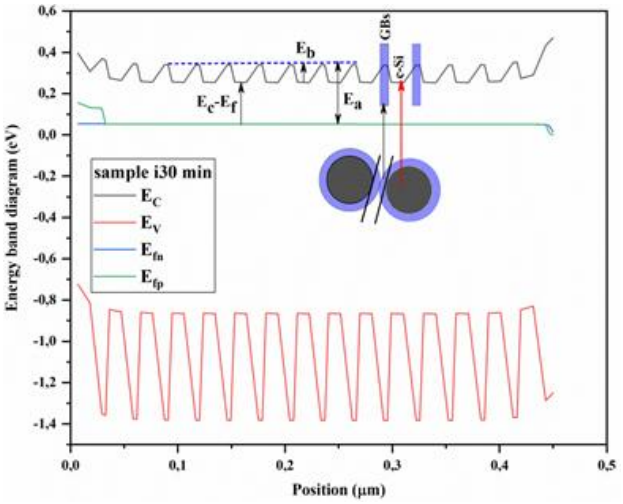

Fig. 8 – Band diagram example of model structure

Amorphous regions create a barrier potential GB between two crystalline regions. The heights of the GB potential barriers of each sample are not constant. The GBs width vary in the range of 2.5 nm till 7 nm [36, 58]. The barrier heights were different at different interfaces depending on varying density of defect states at every GB, as depicted in Fig. 8. Several models have been presented to comprehensive and rationalize the carriers transport mechanism happened at the interface between two materials in order to identify and optimize this contact or activation energy. In terms of classical semiconductor theory, the carriers concentration n_0 and the conductivity σ can be written as [3, 20, 59]:

$$n_0 \propto exp\,[-(E_C - E_f)/kT] \tag{3.1}$$

$$\sigma = n_0 q \mu_H \propto exp\,[-(E_C - E_f)/kT] x exp\,[-E_b/kT] \propto exp\,[-(E_C - E_f + E_b)/kT] \tag{3.2}$$

Therefore, the activation energy is $E_a = E_C - E_f + E_b$ as indicated in Fig. 8. It can be seen from Fig. 8 that the conduction band offset represents the potential barrier height $E_b$of the grain boundaries written in the equation of conductivity. Its value, undoped case, can be well estimated from the curve showing in the Fig. 8, E_b = 0.08 eV. The energy difference value between the Fermi level and the top of the potential barrier is approximately $E_C - E_f$ = 0.038 eV. Therefore, the conductivity activation energy is E_a~0.12 eV.

The Table 1 above shows a comparison of the activation energy estimated from the energy band diagram and the one estimated from the dark current characteristics. The samples n03min of (E_a = 0.12 eV) and n30min

of (E_a = 0.14 eV) clearly indicate that the activation energy obtained with this structure is nearly constant over all bias range and these values differ from the actual conduction band discontinuity ΔE_C only by a few orders of magnitude meV. It is well known that the activation energy of crystalline silicon and their amorphous silicon tissue counterparts were considered to be a half of optical band gap [23].

In previous work [3, 60], these values are the activation energy which corresponds to the potential energy barrier height. This later represents the height of the CB discontinuity in an *a*-Si/*c*-Si heterostructure. Besides, no experimental verification of the barrier height is available to date. Usually, The phenomenon of tunneling mechanism through the interfaces has seldom been introduced in the simulation of the solar cell [61]. However, there are some simulation works that take into account the importance of the tunneling process across contacts [62]. As was stated in the section 2, wxAMPS version has the capabilities to include several different tunneling mechanisms. This end helps to interpret that the tunneling current across the junction interfaces is much more important in these structures for low bias as indicated in the Fig. 9a, where the tunneling process across the conduction band offset may be a realistic scenario.

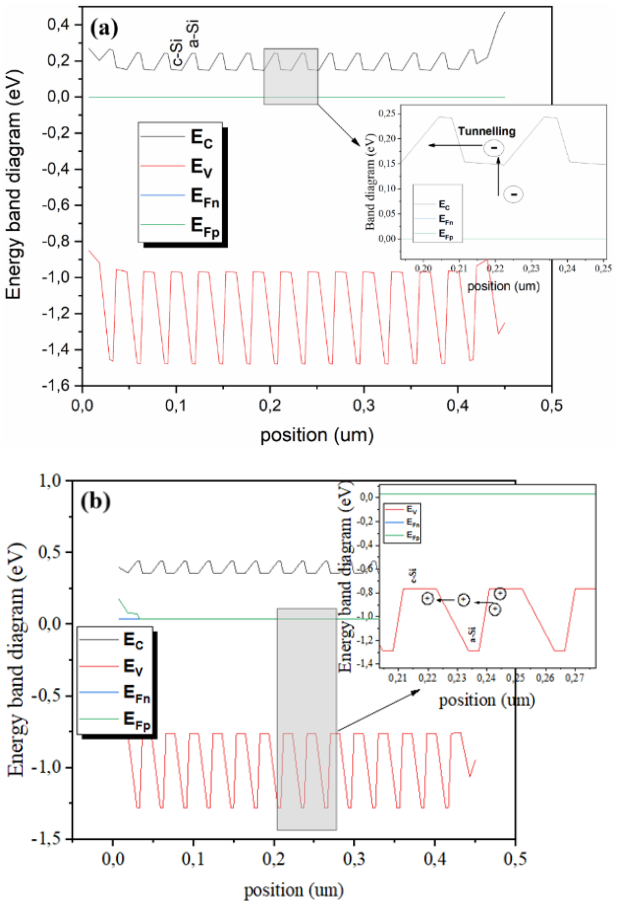

Fig. 9 – Band line-up of the *a*-Si/*c*-Si contact. a) *n*-type nc-Si:H: Electrons generated in the *c*-Si can traverse through the barrier potential (conduction band discontinuity ΔE_C) by tunnel hopping. b) *p*-type nc-Si:H: Holes generated in the *c*-Si can traverse through the Valence band discontinuity ΔE_V by tunnel hopping

Table 2 – Different energy levels electrical calculated from energy band diagram

Sample	$E_C - E_f$ (eV)	E_b(eV) or ΔE_C	E_a(eV)
i03min	0.038	0.08	0.12
n03min	~ 0.12	~ 0.10	0.12
n30min	0.054	0.140	0.14
p03min	–	–	0.18
p30min	–	–	0.216

The samples p03min and p30min of activation energy values E_a = 0.18 eV and E_a = 0.216 eV respectively are calculated from the energy band diagrams. These results also are comparable with the ones calculated from the dark current characteristics. In the Silicon Heterojunction (SHJ), it is well known that the thermionic emission is considered as the main transport mechanism used in the simulation studies of silicon heterojunctions [62]. But the findings reported in the Table 1 above strongly indicate another transport path. Kanevce and Metzger discussed the carriers transport process through the contact between the *n*-type *a*-Si:H and *p*-type *c*-Si layers in detail. Their results clearly demonstrated that an important fraction of the current was derived from tunneling into and tunneling hopping in the layer of *a*-Si:H [61]. In contrast, simulations that include tunnel hopping in *a*-Si:H, or its alloys show good agreement with the experimental data [12]. In fact, some simulation works that clearly illustrate a considerable importance to tunneling across the contact or tunnel hopping in valence band tail states in the *a*-Si:H film as demonstrated in the Fig. 9b [61, 62]. Although, the exact understanding of carrier mechanism is still a subject of discussion and challenge as described by [62].

4. CONCLUSION

In this paper, the dark current mechanisms of nc-Si:H is theoretically and experimentally studied. A complete dark current model considering tunneling mechanism under low bias is constructed. Intrinsic, B and P doped nanocrystalline films, with different crystalline fraction were simulated by assuming them as an alternating of *a*-Si:H and *c*-Si layers. It generates JVT characteristics of the device which show a good agreement with the experimental data.

An analysis of the behavior of the dark JVT curve and the processes involved in the operation of the solar cells was carried out based on the interpretation of the main extracted parameter, E_a. Its values were found, in simulation and experimental, in the range of 0.12 to 0.20 eV. According to these values, the electronic transport mechanism in the films is attributed to the potential barriers that occur at the heterojunction interfaces. These results suggest that the nc-Si:H with a wide range of structure in a given voltage is mainly dominated by a tunneling mechanism: Variable Range Hopping 'VRH' type, or Mott's conductivity instead of the thermal activation model. The good agreement between the simulated and experimental findings observed for different samples confirms the validity of this approach. Doped nc-Si:H samples show a remarkable difference in the dark JVT characteristic compared to the intrinsic ones. P dopant impurities improve further ordered of

nc-Si:H films and therefore high conductivity but the B dopant impurities show the opposite trend; low crystallinity fraction in nc-Si:H and low conductivity.

AKNOWLEDGEMENTS

The authors would like to thank Prof. Yiming Liu at Nankai University for providing wxAMPSand its batch simulation console, and Prof. Stephan Fonash at Pennsylvania State University for the user manual of AMPS. We express our profound gratitude to the Ministry of Higher Education and Scientific Research of Algeria (MESRS) for their valuable support through the national projects: B00L01UN380120220001 and A26N01EP310220230001.

DECLARATION OF COMPETING INTEREST

The authors declare that they have no known competing financial interests or personal relationships that could have appeared to influence the work reported in this paper.

DATA AVAILABILITY

Data will be made available on request.

AUTHORSHIP CONTRIBUTION STATEMENT

All authors contributed equally to this work.

REFERENCES

1. S. Vepřek, V. Mareček, *Solid-State Electron.* **11** No 7, 683 (1968) https://doi.org/10.1016/0038-1101(68)90071-3.
2. D. Shan, Y. Cao, R. Yang, H. Wang, T. Tao, *J. Nanomater.* **2020**, 1 (2020) https://doi.org/10.1155/2020/3698543.
3. D. Shan, M. Qian, Y. Ji, X. Jiang, J. Xu, K. Chen, *Nano-Mater.* **6** No 12, 233 (2016) https://doi.org/10.3390/nano6120233.
4. H.N. Liu, Y.L. He, F. Wang, S. Grebner, *J. Non-Cryst. Solids* **164-166**, 1005 (1993) https://doi.org/10.1016/0022-3093(93)91168-3.
5. R.K. Tripathi, O.S. Panwar, I. Rawal, B.P. Singh, B.C. Yadav, *J. Taiwan Inst. Chem. Eng.* **86**, 185 (2018) https://doi.org/10.1016/j.jtice.2018.01.051.
6. B. Garrido, A. Pérez-Rodríguez, J.R. Morante, A. Achiq, F. Gourbilleau, R. Madelon, R. Rizk, *J. Vac. Sci. Technol. B Microelectron. Nanometer Struct. Process. Meas. Phenom.* **16** No 4, 1851 (1998) https://doi.org/10.1116/1.590097.
7. W. Wei, G. Xu, T. Wang, W.Z. Shen, *Thin Solid Films* **515** No 7-8, 3997 (2007) https://doi.org/10.1016/j.tsf.2006.09.052.
8. X. Zhang, G. Han, *Thin Solid Films* **415** No 1-2, 5 (2002) https://doi.org/10.1016/S0040-6090(02)00503-5.
9. Z.A.K. Durrani, M.A. Rafiq, *Microelectron. Eng.* **86** No 4-6, 456 (2009) https://doi.org/10.1016/j.mee.2009.03.123.
10. C. Gonçalves, S. Charvet, A. Zeinert, M. Clin, K. Zellama, *Thin Solid Films* **403-404**, 91 (2002) https://doi.org/10.1016/S0040-6090(01)01553-X.
11. M. Morales, Y. Leconte, R. Rizk, D. Chateigner, *J. Appl. Phys.* **97** No 3, 034307 (2005) https://doi.org/10.1063/1.1841461.
12. D. Benlakehal, A. Belfedal, Y. Bouizem, J.D. Sib, L. Chahed, K. Zellama, *Superlattice. Microst.* **100**, 228 (2016) https://doi.org/10.1016/j.spmi.2016.09.035.
13. M. Kondo, A. Matsuda, *Thin-Film Sol. Cells, Preparation and Properties of Nanocrystalline Silicon* (Berlin, Heidelberg: Springer Berlin Heidelberg: 2004).
14. M. Sharma, J. Panigrahi, V.K. Komarala, *Nanoscale Adv.* **3** No 12, 3373 (2021) https://doi.org/10.1039/D0NA00791A.
15. S. El Whibi, L. Derbali, P. Tristant, C. Jaoul, M. Colas, R. Mayet, J. Cornette, H. Ezzaouia, *J. Mater. Sci. Mater. Electron.* **30** No 3, 2351 (2019) https://doi.org/10.1007/s10854-018-0508-9.
16. J.J. Lu, J. Chen, Y.L. He, W.Z. Shen, *J. Appl. Phys.* **102** No 6, 063701 (2007) https://doi.org/10.1063/1.2779267.
17. M. Anutgan, S. Uysal, T. Anutgan, *Eur. Phys. J. Appl. Phys.* **65** No 2, 20301 (2014) https://doi.org/10.1051/epjap/2013130394.
18. D. Cavalcoli, F. Detto, M. Rossi, A. Tomasi, A. Cavallini, *Nanotechnology* **21** No 4, 045702 (2010) https://doi.org/10.1088/0957-4484/21/4/045702.
19. B. Yan, G. Yue, J. Yang, S. Guha, *Sol. Energy Mater. Sol. C.* **111**, 90 (2013) https://doi.org/10.1016/j.solmat.2012.12.038.
20. G. Xiao-Yong, Z. Jian-Tao, L. Yu-Fen, L. Qing-Geng, C. Yong-Sheng, G. Jin-Hua, Y. Shi-E, L. Jing-Xiao, *Acta Phys. Pol. A* **115** No 3, 738 (2009) https://doi.org/10.12693/APhysPolA.115.738.
21. W. Fuhs, *J. Non-Cryst. Solids* **354** No 19-25, 2067 (2008) https://doi.org/10.1016/j.jnoncrysol.2007.09.008.
22. C. Patra, D. Das, *Mater. Today Proc.* **62**, 5110 (2022) https://doi.org/10.1016/j.matpr.2022.02.456.
23. B. Rezek, J. Stuchlík, A. Fejfar, J. Kočka, *J. Appl. Phys.* **92** No 1, 587 (2002) https://doi.org/10.1063/1.1486032.
24. C. Ross, J. Herion, H. Wagner, *J. Non-Cryst. Solids* **266-269**, 69 (2000) https://doi.org/10.1016/S0022-3093(99)00736-X.
25. D. Azulay, I. Balberg, V. Chu, J.P. Conde, O. Millo, *Phys. Rev. B* **71** No 11, 113304 (2005) https://doi.org/10.1103/PhysRevB.71.113304.
26. P. Abboud, F. Martinez, R. Amrani, D. Habib, S. Parola, Y. Cuminal, *J. Non-Cryst. Solids* **477**, 42 (2017) https://doi.org/10.1016/j.jnoncrysol.2017.09.045.
27. I. Balberg, Y. Dover, R. Naides, J.P. Conde, V. Chu, *Phys. Rev. B* **69** No 3, 035203 (2004) https://doi.org/10.1103/PhysRevB.69.035203.
28. M. Chahi, A. Bouhekka, J.D. Sib, A. Kebab, Y. Bouizem, L. Chahed, *Phys. Status Solidi C* **7** No 3-4, 640 (2010) https://doi.org/10.1002/pssc.200982691.
29. S. Tripathi, N. Venkataramani, R.O. Dusane, B. Schroeder, *Thin Solid Films* **501** No 1-2, 295 (2006) https://doi.org/10.1016/j.tsf.2005.07.199.
30. G.Y. Hu, R.F. O'Connell, Y.L. He, M.B. Yu, *J. Appl. Phys.* **78** No 6, 3945 (1995) https://doi.org/10.1063/1.359914.
31. Y. Liu, D. Heinzel, A. Rockett, *2010 35th IEEE Photovolt. Spec. Conf., A revised version of the AMPS simulation code* (Honolulu, HI, USA: IEEE: 2010).
32. D. Senouci, R. Baghdad, A. Belfedal, L. Chahed, X. Portier, S. Charvet, K.H. Kim, P. Roca I Cabarrocas, K. Zellama, *Thin Solid Films* **522**, 186 (2012) https://doi.org/10.1016/j.tsf.2012.08.014.
33. Z.A.K. Durrani, H. Ahmed, *Nanosilicon, Nanosilicon Single-Electron Transistors and Memory* (Elsevier: 2008).
34. P.G. Lecomber, G. Willeke, W.E. Spear, *J. Non-Cryst. Solids* **59-60**, 795 (1983) https://doi.org/10.1016/0022-3093(83)90290-9.
35. J.Y.W. Seto, *J. Appl. Phys.* **46** No 12, 5247 (1975) https://doi.org/10.1063/1.321593.
36. P. Dutta, M. Kumar, M. Rathi, S.P. Ahrenkiel, S. Paul, D. Galipeau, V. Bommisetty, *J. Nanosci. Nanotechnol.* **13** No 10, 6711 (2013) https://doi.org/10.1166/jnn.2013.7783.

37. Y. Liu, Y. Sun, A. Rockett, *Sol. Energy Mater. Sol. C.* **98**, 124 (2012) https://doi.org/10.1016/j.solmat.2011.10.010.
38. S. Yaşar, S. Kahraman, S. Çetinkaya, Ş. Apaydın, İ. Bilican, İ. Uluer, *Optik* **127** No 20, 8827 (2016) https://doi.org/10.1016/j.ijleo.2016.06.094.
39. J. Smucker, J. Gong, *Sol. Energy* **228**, 187 (2021) https://doi.org/10.1016/j.solener.2021.09.066.
40. J. Kanicki, *Amorphous and Microcrystalline Semiconductor Devices* (Boston: Artech House: 1991).
41. A. Jüngel, *Transport Equations for Semiconductors* (Berlin, Heidelberg: Springer Berlin Heidelberg: 2009).
42. S.S. Hegedus, W.N. Shafarman, *Prog. Photovolt. Res. Appl.* **12** No 2-3, 155 (2004) https://doi.org/10.1002/pip.518.
43. S.B. Concari, R.H. Buitrago, M.T. Gutiérrez, J.J. Gandía, *J. Appl. Phys.* **94** No 4, 2417 (2003) https://doi.org/10.1063/1.1593215.
44. P. Nagels, *Amorph. Semicond., Electronic Transport in Amorphous Semiconductors* (Berlin, Heidelberg: Springer Berlin Heidelberg: 1979).
45. M.H. Gullanar, Y.H. Zhang, H. Chen, W.S. Wei, G.Y. Xu, T.M. Wang, R.Q. Cui, W.Z. Shen, *J. Cryst. Growth* **256** No 3-4, 254 (2003) https://doi.org/10.1016/S0022-0248(03)01371-X.
46. D. Li, J. Xu, P. Zhang, Y. Jiang, K. Chen, *J. Phys. Appl. Phys.* **51** No 23, 233002 (2018) https://doi.org/10.1088/1361-6463/aac1fe.
47. P.G. Le Comber, *Sci. Prog.* **66** No 261, 105 (1979).
48. N.F. Mott, E.A. Davis, R.A. Street, *Philos. Mag.* **32** No 5, 961 (1975) https://doi.org/10.1080/14786437508221667.
49. Yuqing Huang, J. Liu, J. Wang, D. Bao, S. Huang, *Surf. Eng. Appl. Electrochem.* **55** No 3, 259 (2019) https://doi.org/10.3103/S1068375519030098.
50. D. Das, K. Bhattacharya, *J. Appl. Phys.* **100** No 10, 103701 (2006) https://doi.org/10.1063/1.2384812.
51. I. Balberg, J. Jedrzejewski, E. Savir, *Phys. Rev. B* **83** No 3, 035318 (2011) https://doi.org/10.1103/PhysRevB.83.035318.
52. M. Khelil, S. Kraiem, M. Kraini, C. Vázquez-Vázquez, K. Khirouni, M.A. López-Quintela, *J. Mater. Sci. Mater. Electron.* **29** No 13, 11000 (2018) https://doi.org/10.1007/s10854-018-9182-1.
53. D. Das, B. Sain, *J. Appl. Phys.* **114** No 7, 073708 (2013) https://doi.org/10.1063/1.4818512.
54. G. Blaise, *J. Electrost.* **50** No 2, 69 (2001) https://doi.org/10.1016/S0304-3886(00)00027-9.
55. M.A. Majeed Khan, M. Zulfequar, M. Husain, *Curr. Appl. Phys.* **2** No 5, 401 (2002) https://doi.org/10.1016/S1567-1739(02)00148-7.
56. M.D.K. Jones, J.A. Dawson, S. Campbell, V. Barrioz, L.D. Whalley, Y. Qu, *Front. Chem.* **10**, 920676 (2022) https://doi.org/10.3389/fchem.2022.920676.
57. S.J. Konezny, M.N. Bussac, L. Zuppiroli, *Appl. Phys. Lett.* **92** No 1, 012107 (2008) https://doi.org/10.1063/1.2828991.
58. T. Dinh, D.V. Dao, H.-P. Phan, L. Wang, A. Qamar, N.-T. Nguyen, P. Tanner, M. Rybachuk, *Appl. Phys. Exp.* **8** No 6, 061303 (2015) https://doi.org/10.7567/APEX.8.061303.
59. L.-P. Scheller, N.H. Nickel, *J. Appl. Phys.* **112** No 1, 013713 (2012) https://doi.org/10.1063/1.4733699.
60. A. Kanevce, W.K. Metzger, *J. Appl. Phys.* **105** No 9, 094507 (2009) https://doi.org/10.1063/1.3106642.
61. M. Mews, M. Liebhaber, B. Rech, L. Korte, *Appl. Phys. Lett.* **107** No 1, 013902 (2015) https://doi.org/10.1063/1.4926402.
62. Y. Liu, Y. Sun, A. Rockett, *Thin Solid Films* **520** No 15, 4947 (2012) https://doi.org/10.1016/j.tsf.2012.03.012.

wxAMPS-моделювання механізму електронного переносу у власних та легованих нанокристалічних кремнієвих тонких плівках

M. Chahi[1,2], A. Gharou[3], H. Nehmar[4], M. Kasdi[3], H. Benhabara[4], A. Bouhekka[3,4]

[1] *Laboratoire de Génie Electrique et Matériaux LGEM Ecole Supérieure en Génie Electrique et Energétique ESGEE d'Oran, Oran, Algeria*

[2] *Institute of Nature and Life Sciences, Tissemsilt University – Ahmed Ben Yahia ELWancharissi, P.B. 182 Bougara Road, 38000 Tissemsilt, Algeria*

[3] *Department of Matter Sciences, Faculty of Sciences and Technology, Tissemsilt University – Ahmed Ben Yahia ELWancharissi, P.B. 182 Bougara Road, 38000 Tissemsilt, Algeria*

[4] *Laboratoire de Physique des Couches Minces et Matériaux pour l'Electronique – LPCMME, Université Oran 1 Ahmed Ben Bella, B.P. 1524, El M'naouar 31100 Oran, Algeria*

Представлено числове дослідження транспортних властивостей у тонких плівках гідрогенізованого нанокристалічного кремнію для сонячних елементів за допомогою програмного забезпечення wxAMPS. Модельовані зразки були виготовлені при температурі 100 °C за допомогою методу радіочастотного магнетронного розпилення (RFMS) з потужністю радіочастотного випромінювання 220 Вт, газової суміші з 30 % аргону та 70 % водню під загальним тиском 3 Па, а відстань між мішенню та тримачем зразка, фіксована на рівні 70 мм, підтримувалася постійною для трьох категорій власних плівок, легованих фосфором та легованих бором, при часі осадження 3 та 30 хвилин. Моделювання, проведене в цьому дослідженні, базується на шарі нанокристалічного кремнію, який був побудований з використанням послідовних та альтернативних тонких кристалічних та аморфних шарів, де їх загальна кількість залежить від товщини досліджуваного зразка. Досліджено механізм електронного транспорту, і результати чітко показали, що леговані та нелеговані зразки мають різну енергію активації (E_a), що очевидно ілюструє вирішальну роль легування. E_a менше 0,2 еВ для всіх модельованих зразків, що чітко вказує на механізм транспорту з надією. Ці результати порівняли з експериментальними та попередніми роботами, де спостерігалася добра узгодженість.

Ключові слова: Нанокристалічний кремній, Програмне забезпечення wxAMPS, Темнова провідність, Енергія активації, Стрибок, Моделювання.